Inorganic Chemistry

ARTICLE

pubs.acs.org/IC

Capture of the Complex $[Ni(dto)_2]^{2-}$ (dto^{2-} = Dithiooxalato Ligand) in a Mo_{12} Ring: Synthesis, Characterizations, and Application toward the Reduction of Protons

Akram Hijazi,[†] Justin Claude Kemmegne-Mbouguen,[†,‡] Sébastien Floquet,*[,†] Jérôme Marrot,[†] Cédric R. Mayer,[†] Vincent Artero,[§] and Emmanuel Cadot[†]

[†]Institut Lavoisier de Versailles, UMR 8180, Université de Versailles Saint-Quentin en Yvelines, 45 avenue des Etats-Unis, 78035 Versailles, France

[‡]Laboratoire de Chimie Analytique, Faculté des Sciences, Université de Yaoundé I, B.P. 812, Yaoundé, Cameroon

[§]Laboratoire de Chimie et Biologie des Métaux, UMR 5249, Université Joseph Fourier, Grenoble 1−CNRS−CEA, 17 rue des Martyrs, 38054 Grenoble Cedex 9, France

Supporting Information

ABSTRACT: The encapsulation of the complex $[Ni(dto)_2]^{2-}$ within an oxothiododecamolybdic cyclic cluster has been investigated. The resulting molybdenum ring, $[Mo_{12}O_{12}S_{12}(OH)_{12}(Ni(dto)_2)]^{2-}$, corresponds to the first example of the $\{Mo_2O_2S_2\}$-based assembly arranged around a 3d transition-metal complex. It was unambiguously characterized in the solid state and in solution by FT-IR spectroscopy, single-crystal X-ray diffraction, NMR, UV−visible spectroscopy, and electrospray ionization-high-resolution mass spectrometry (ESI-HRMS). The latter technique revealed to be a powerful tool for the characterization of templated molybdenum ring systems in solution and gave excellent results in high resolution. The electronic spectrum of $[Mo_{12}O_{12}S_{12}(OH)_{12}(Ni(dto)_2)]^{2-}$ evidenced a strong red shift of the LMCT bands attributed to the complex $[Ni(dto)_2]^{2-}$, suggesting significant variations of the electronic properties upon its encapsulation within the Mo_{12} ring. These differences were demonstrated by electrochemical studies in CH_3CN, which also revealed, for both compounds $[Ni(dto)_2]^{2-}$ and $[Mo_{12}O_{12}S_{12}(OH)_{12}(Ni(dto)_2)]^{2-}$, electrocatalytic properties for the reduction of protons. These results evidence the ability of dithioxalato complexes to act as electrocatalysts for the hydrogen evolution reaction (HER) and confirm such a property for oxothiomolybdenum rings.

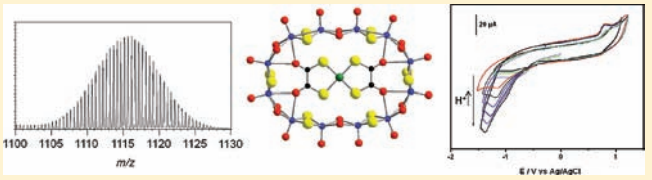

INTRODUCTION

Dithiooxalate (denoted dto^{2-}) complexes of transition metals have been known for a century[1−3] and have been widely studied because of their various properties in catalysis, optics, or in magnetism. This ditopic ligand is usually coordinated to transition metals by sulfur atoms, and the external oxalate moieties are available for additional coordination with 3d or 4f elements to lead to discret polymetallic complexes[4−7] or infinite materials.[8−14] This propensity to give heterometallic chains or materials was especially developed for magnetic and/or optical properties. Among this family of complexes, the compound $[Ni(dto)_2]^{2-}$ is probably one of the most studied since its first publication in 1909. This complex retains a square-planar geometry within a NiS_4 coordination sphere, which is comparable to the environment of the Ni center in NiFe hydrogenases.[15−25] Besides, some recent results revealed that some Nickel clusters formed with sulfur-containing ligands are efficient for proton reduction into hydrogen,[26] a behavior that was not yet evidenced for dto^{2-} complexes to our knowledge.

This domain of research receives a growing interest because molecular hydrogen is strongly envisioned as a clean energy carrier for the future. In this field, we recently evidenced that oxothiomolybdenum rings are able to function as efficient electrocatalysts toward the reduction of protons into hydrogen (HER) both in organic and in aqueous media.[27,28] This wide class of compounds is based on the self-condensation of $[M_2O_2S_2]^{2+}$ oxothiocations ($M = Mo^V, W^V$) around anionic templates, being either mono- or polyphosphates,[29] metalates,[30] or polycarboxylates.[27,31−36] Trends in electrocatalytic properties for this class of molecular materials are not well-understood, but their chemical potentialities, based upon the diversity of the host−guest combinations, should offer some relevant optimization perspectives. One idea consists of including electroactive transition-metal complexes within the Mo ring with the aim to induce some synergistic functionalities, such as electrons/protons storage or transfer. The tremendous propensity of the Mo rings to encapsulate polycarboxylate ions prompts us recently to use the $[Mo_3S_4(nta)_3]^{5-}$ anionic cluster as a guest component (nta^{3-} = nitrilotriacetate), thus leading to a spectacular electroactive Mo_{18} ring assembled around the three

Received: June 9, 2011
Published: August 02, 2011

Scheme 1

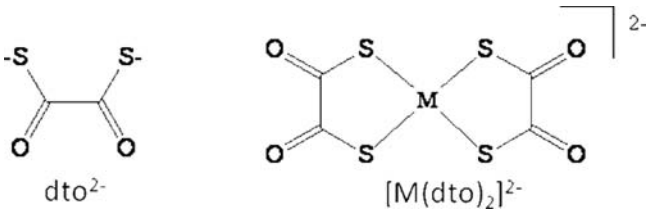

hanging carboxylate functions of $[Mo_3S_4(nta)_3]^{5-}$.[27] In the same step, we report herein the synthesis and the characterization of a new dodecamolybdenum wheel self-assembled around the anionic complex $[Ni(dto)_2]^{2-}$, the first example of a 3d transition metal embedded in the plane of the Mo ring (see Scheme 1). The resulting compound $[Mo_{12}{-}Ni(dto)_2]^{2-}$ was characterized by X-ray diffraction study and spectroscopic methods, especially ESI-HRMS. Furthermore, the electrochemical behavior was investigated, showing that both compounds $[Ni(dto)_2]^{2-}$ and $[Mo_{12}(Ni(dto)_2)]^{2-}$ are active toward the reduction of protons.

EXPERIMENTAL SECTION

Physical Methods. Infrared spectra were recorded on a Magna 550 Nicolet spectrophotometer, using KBr pellets. NMR measurements were performed on a Bruker Avance 300 operating at 300 MHz for ^{1}H in 5 mm tubes. Chemical shifts were referenced to the usual external TMS standard. Elemental analyses were performed by the Service Central D'Analyses du CNRS, Vernaison, France, or by the Service D'Analyses du CNRS, ICSN, Gif sur Yvette, France. EDX measurements were performed on a JEOL JSM 5800LV apparatus. Spectrophotometric studies were carried out on a PerkinElmer Lambda 19 spectrophotometer, at room temperature by using quartz cells with a 1 mm path length. Electrospray ionization-mass spectrometry (ESI-MS) routine spectra were carried out at the University of Paris XI Orsay (ICMMO) with a Thermo Scientific TSQ apparatus. Electrospray ionization-high-resolution mass spectrometry (ESI-HRMS) measurements were carried out with a Waters Xevo-QTOF. The experiments were performed with the negative ion mode in acetonitrile by direct infusion with a syringe pump with a flow rate of 5 μL·min^{-1}. Standard experimental conditions were the following: sample concentration, 6×10^{-6} M; leucine encephaline as external calibrate; capillary high voltage, 1.2 kV; extraction cone, 3.0 V; sampling cone, 15 V; temperature source, 100 °C; and temperature desolvation, 300 °C. Cyclic voltammetric (CV) experiments were carried out in dry acetonitrile with an Autolab PGSTAT12 potentiostat/galvanostat associated with a GPES electrochemical analysis system (EcoChemie). Measurements were performed at room temperature in a conventional single compartment cell with a Ag/AgCl reference electrode, platinum gauze with a large surface area, and a static glassy carbon disk working electrode (GCE). The source, mounting, and polishing of the glassy carbon electrodes (ø 3 mm) have been described previously.[37] The solutions were deaerated thoroughly for at least 30 min with pure argon and kept under a positive pressure of this gas during the experiments. For bulk electrolysis experiments, a tight cell was used, with the platinum-grid counter electrode placed in a separate compartment connected by a glass frit and filled with the electrolytic solution. The working electrode was a glassy carbon rod (Neyco, 10 mm in diameter). A degassed CH_3CN solution (10 mL) containing 0.1 mol·L^{-1} (n-Bu_4N)PF_6 and CF_3COOH (TFA, 1.5 mmol·L^{-1}) was electrolyzed at −1.40 V vs Ag/AgCl for 2 h in the absence or in the presence of the catalyst (1 μmol). During these controlled-potential Coulometry experiments, the cell was flushed with nitrogen (5 mL·min^{-1}) and the output gas was sampled (100 μL) every 2 min and analyzed using a PerkinElmer Clarus 500 gas chromatograph equipped with a porapack Q 80/100 column (6′ 1/8″) thermostatted at 40 °C and a TCD detector thermostatted at 100 °C. Note that, for the electrochemical studies, the TFA solutions were prepared in CH_3CN by using 99% commercial TFA and dry acetonitrile, thus strongly limiting the addition of water through increasing adducts of acid to **1** or **2**.

Syntheses. $K_{2-x}(NMe_4)_x[I_2Mo_{10}O_{10}S_{10}(OH)_{10}(H_2O)_5]\cdot 20H_2O$ ($0 < x < 0.5$) was prepared as described in the literature and characterized by routine methods.[38] Thiophenol, oxalylchloride, and metallic salts were purchased from Aldrich Chemicals, whereas potassium hydrogenosulfide was provided by Strem Chemicals.

K_2dto and Potassium Dithiooxalatonickelate(II), $K_2[Ni(dto)_2]\cdot H_2O$, ***K-1***. The ligand potassium dithiooxalate was prepared in two steps according to the method of Jones and Tasker.[3] The synthesis of **K-1** was inspired from Jones and Robinson[1] and Cox et al.,[39,40] and experimental details are given in the Supporting Information.

$(PPN)_2[Ni(dto)_2]$, ***PPN-1***. The bis(triphenylphosphoranylidene)-ammonium (PPN^+) salt of **1** was prepared by metathesis of **K-1**. To a solution of **K-1** (200 mg, 0.5 mmol) in water (5 mL) was added an aqueous solution of PPNCl in excess (0.75 g, 1.25 mmol in 10 mL of water). The corresponding $(PPN)_2[Ni(dto)_2]$ complex (ca. 0.7 g, yield about 100%) was isolated by filtration and recrystallized in CH_3CN (25 mL) by slow addition of *tert*-butyl methyl ether to give single-crystals suitable for X-ray diffraction study (0.4 g; yield, 58%). FT-IR/cm^{-1}, (KBr pellet): 1593 (s), 1585 (ms), 1436 (m, PPN^+), 1219 (s, PPN^+), 1115 (ms), 1053 (m), 722 (m, PPN^+), 690 (m, PPN^+), 551 (m, PPN^+), 535 (m, PPN^+), 503 (m, PPN^+). ESI-MS (CH_3CN): m/z = 149.9 (expected: m/z = 149.5). ^{13}C NMR in CD_3CN: 199.3 ppm. EDX atomic ratios calculated for $(P_2NC_{36}H_{30})_2[Ni(C_2S_2O_2)_2]$ (found): P/Ni = 4.0 (4.01), S/Ni = 4.0 (4.17). Elemental analysis calcd (%) for $(P_2NC_{36}H_{30})_2[Ni(C_2S_2O_2)_2]$ (M = 1376.2 g mol^{-1}): C, 66.33; H, 4.39; N, 2.04; S, 9.32. Found: C, 66.28; H, 4.41; N, 2.17; S, 9.55.

$Rb_2[Mo_{12}O_{12}S_{12}(OH)_{12}(Ni(dto)_2)]\cdot 2CH_3CN\cdot 20H_2O$, ***Rb-2***. $K_{2-x}(NMe_4)_x[I_2Mo_{10}O_{10}S_{10}(OH)_{10}(H_2O)_5]\cdot 20\ H_2O$ (230 mg, 0.096 mmol, 0.08 mmol of Mo_{12}) was suspended in water (10 mL) and **K-1** (32 mg, 0.08 mmol) was dissolved in water (5 mL). The mixing of both reactants gave a purple solution with a pH value about 4. This resulting solution was stirred for 30 min at room temperature before centrifugation (10 000 rpm for 5 min) to remove a cloudy precipitate. Rubidium chloride (1 g, 8.26 mmol) was then added to the clear filtrate to give a dark purple solid that was isolated by filtration, washed with cold water, ethanol, and ether, and dried in air. The crude product was dissolved in the minimum volume of acetonitrile (ca. 20 mL) for purification. After filtration, the clear purple solution was evaporated slowly in air at room temperature until a dry solid was obtained. Yield: 180 mg (79%). FT-IR/cm^{-1}, (KBr pellet): 1609 (m), 1529 (sh), 1513 (s), 1102 (m), 960 (vs), 515 (s), 422 (w), 339 (m). ^{1}H NMR in DMSO (δ/ppm): 10.85 (s, 8H), 10.69 (s, 4H). NMR ^{1}H (CD_3CN/ppm): 8.77 (s, 8H), 8.53 (s, 4H). ESI-HRMS (CH_3CN): m/z = 1115.59 (expected: m/z = 1115.65). Elemental analysis calcd (%) for $Rb_2[Mo_{12}O_{12}S_{12}(OH)_{12}(Ni(C_2S_2O_2)_2)]\cdot 20H_2O\cdot 2CH_3CN$ (M = 2844.5 g mol^{-1}): C, 3.38; H, 2.06; N, 0.98; S, 18.04; Ni, 2.06. Found: C, 3.33; H, 1.95; N, 0.87; S, 18.10; Ni, 2.23.

$(PPN)_2[Mo_{12}O_{12}S_{12}(OH)_{12}(Ni(dto)_2)]\cdot 11DMF\cdot 2H_2O$. ***PPN-2·DMF***. $K_{2-x}(NMe_4)_x[I_2Mo_{10}O_{10}S_{10}(OH)_{10}(H_2O)_5]\cdot 20\ H_2O$ (294 mg, 0.12 mmol) was suspended in water (12 mL). **K-1** (40 mg, 0.1 mmol) was dissolved in water (5 mL) and then mixed to the former solution. The resulting purple solution (pH = 4.2) was stirred for 30 min at room temperature and centrifuged (10 000 rpm for 5 min) to give a clear solution. PPNCl (ca. 500 mg, 0.87 mmol) was then added to the filtrate, provoking the formation of a dark purple solid, which was isolated by filtration, washed by water, ethanol, and ether to give 400 mg of a crude

dx.doi.org/10.1021/ic201239y |*Inorg. Chem.* 2011, 50, 9031–9038

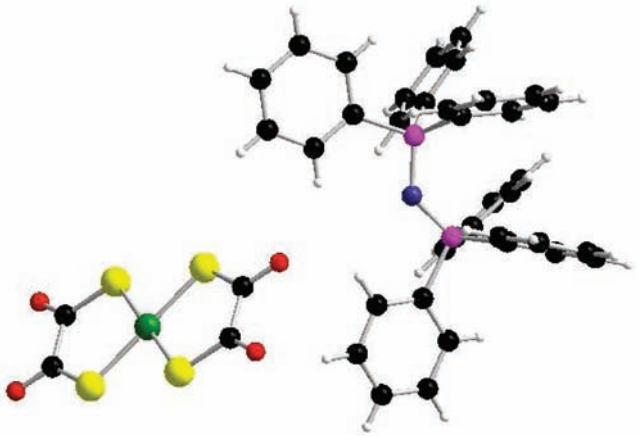

Figure 1. Ball-and-stick representation of **PPN-1**. Color code: oxygen in red, sulfur in yellow, carbon in black, nickel in green, phosphorus in pink, nitrogen in dark blue, and hydrogen in white.

solid material. The latter was dissolved in 20 mL of dry DMF. After 12 h, a crystalline powder of **PPN-2·DMF** was collected by filtration, washed with water, ethanol, and diethyl ether to give 145 mg of **PPN-2·DMF** (yield 35%). FT-IR/cm^{-1}, (KBr pellet): 1654 (vs, DMF), 1541 (s), 1438 (m, PPN$^+$), 1384 (m, DMF), 1258 (br m, PPN$^+$), 1115 (m), 1097 (m, DMF), 970 (vs), 723 (m, PPN$^+$), 691 (m, PPN$^+$), 551 (w, PPN$^+$), 533 (m, PPN$^+$), 525 (s). ^{1}H NMR in DMSO (δ/ppm): 10.84 (s, 8H), 10.68 (s, 4H), 7.95 (s, 11H, DMF), 7.4−7.8 (m, 60H, PPN$^+$), 2.88 (s, 33H, DMF), 2.72 (s, 33H, DMF). Elemental analysis calcd (%) for $(P_2NC_{36}H_{30})_2[Mo_{12}O_{12}S_{12}(OH)_{12}(Ni(C_2S_2O_2)_2)]\cdot 11DMF\cdot 2H_2O$ (M = 4148.4 g mol^{-1}): C, 31.43; H, 3.71; N, 4.52; S, 12.52; Ni, 1.41. Found: C, 31.56; H, 3.72; N, 4.39; S, 12.67; Ni, 1.28.

$(PPN)_2[Mo_{12}O_{12}S_{12}(OH)_{12}(Ni(dto)_2)]\cdot 8CH_3CN\cdot 2.8H_2O\cdot 1.2MeOtbu$. ***PPN-2·CH$_3$CN***. **PPN-2·DMF** (100 mg; 0.024 mmol) was dissolved in 25 mL of acetonitrile, and *tert*-butyl methyl ether was allowed to slowly diffuse into this solution. After one week, small parallelepipedic single crystals of **PPN-2·CH$_3$CN**, suitable for X-ray diffraction analysis, were obtained (ca. 25 mg, yield 27%). FT-IR/cm^{-1}, (KBr pellet): 1616 (w), 1539 (s), 1437 (m, PPN$^+$), 1250 (w, PPN$^+$), 1115 (m), 970 (vs), 723 (m, PPN$^+$), 691 (m, PPN$^+$), 551 (w, PPN$^+$), 533 (m, PPN$^+$), 519 (s).^{1}H NMR in DMSO (δ/ppm): 10.84 (s, 8H), 10.68 (s, 4H), 7.4−7.8 (m, 60H, PPN$^+$). ESI-HRMS (CH_3CN): m/z = 1115.65 (expected: m/z = 1115.65). EDX atomic ratios calculated for $(P_2NC_{36}H_{30})_2[Mo_{12}O_{12}S_{12}(OH)_{12}(Ni(C_2S_2O_2)_2)]$ (found): S/Mo = 1.33 (1.30), Mo/Ni = 12.0 (11.94), Mo/P = 3.0 (2.99), P/Ni = 4.0 (3.99).

RESULTS AND DISCUSSION

Synthesis. The synthesis of the anionic cluster $[Mo_{12}O_{12}S_{12}(OH)_{12}(Ni(dto)_2)]^{2-}$ (**2**) was carried out in water at room temperature and recrystallization achieved in organic media. The resulting complex appears stable enough in aqueous solution to be isolated as a pure compound. Nevertheless, the aged aqueous solutions of **2** revealed the formation of the oxalato Mo ring, denoted $[Mo_8\text{-}ox]^{2-}$ as a byproduct, which was identified easily in the solid state by FT-IR and in solution by ESI-HRMS and ^{1}H NMR. Such a result shows that hydrolysis of the ligand dto^{2-} occurs in aqueous solution, leading to the formation of oxalate ions while the free complex $[Ni(dto)_2]^{2-}$(**1**) is perfectly stable in aqueous medium. The decomposition process of the dto^{2-} ligand becomes predominant for temperatures above 40 °C, and pH up to 4.5 The

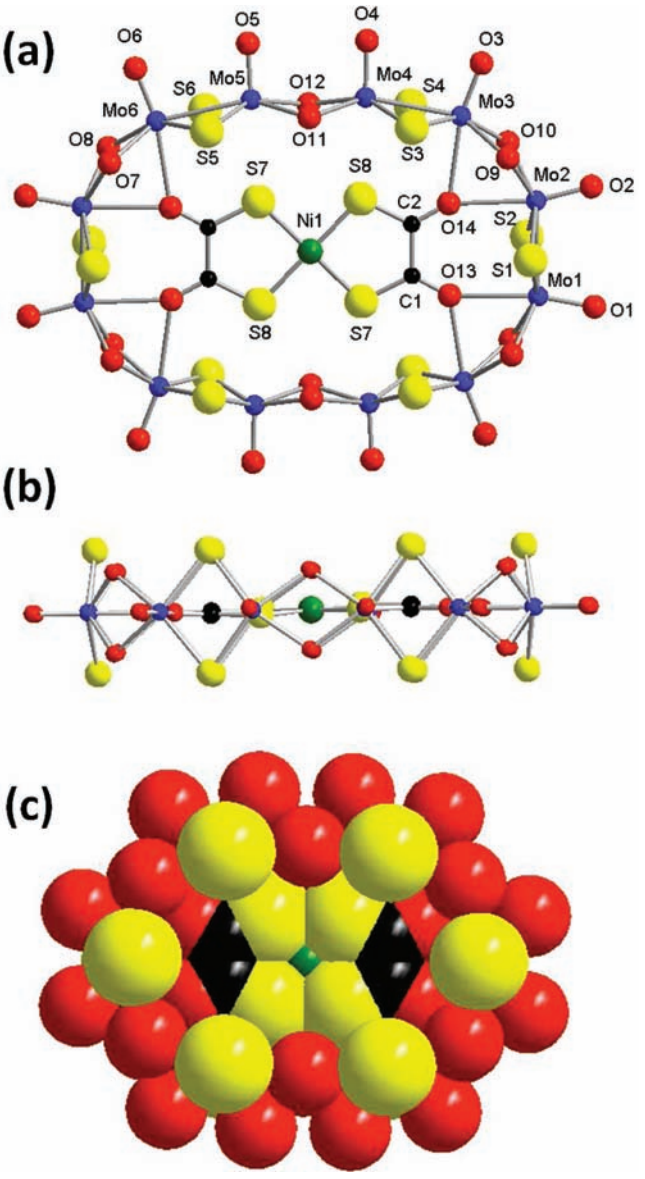

Figure 2. Top (a) and side (b) views of labeled ball-and-stick representations of **2**. Space-filling representation of **2** (c). Color code: Mo in blue, oxygen in red, sulfur in yellow, carbon in black, and nickel in green.

hydrolysis of the dto^{2-} ligand from **2** is no doubt favored by the formation of the highly stable $[Mo_8O_8S_8(OH)_8(C_2O_4)]^{2-}$ compound.[28,35] Consequently, the first step of the synthesis of **2** carried out in an aqueous medium has to be shortened (about 30 min at RT) and compound **2** used in dry solvents.

X-ray Diffraction Studies. The molecular structures of **1** and **2** are depicted in Figures 1 and 2. Crystal data are given in Table 1, whereas selected bond lengths are listed in Table 2.

The structure of **PPN-1** (Figure 1) consists of a discrete $[Ni(dto)_2]^{2-}$ anionic complex associated to two organic PPN$^+$ cations. The Ni−S, C−S, C−C, and C−O distances of the $[Ni(dto)_2]^{2-}$ moiety (see Table 2) are in good agreement with the literature data reported for various salts of $[Ni(dto)_2]^{2-}$.[4,41,42]

PPN-2·CH$_3$CN. A basic description of the molecular architecture of **2** (see Figure 2) consists of a planar guest $[Ni(dto)_2]^{2-}$ anion encapsulated into the cyclic neutral skeleton $[Mo_{12}S_{12}O_{12}(OH)_{12}]$.

dx.doi.org/10.1021/ic201239y |*Inorg. Chem.* 2011, 50, 9031–9038

Table 1. Structural Parameters for Compounds (PPN)-1 and (PPN)-2·CH_3CN

compound	(PPN)-1	(PPN)-2·CH_3CN
empirical formula	$C_{76}H_{60}N_2NiO_4P_4S_4$	$C_{98}H_{116}Mo_{12}N_{10}NiO_{32}P_4S_{16}$
formula weight	1376.09	3792.84
temperature/K	296(2)	200(2)
crystal size/mm	0.25 × 0.20 × 0.10	0.10 × 0.05 × 0.03
crystal system	monoclinic	triclinic
space group	$P2(1)/n$	$P\bar{1}$
a/Å	9.7677(2)	9.7871(10)
b/Å	15.9377(5)	15.8004(15)
c/Å	22.1040(6)	24.637(2)
α/°	90	107.425(5)
β/°	101.4100(10)	92.893(5)
γ/°	90	104.568(5)
V/Å^3	3373.03(16)	3485.3(6)
Z	2	1
D_c/g cm^{-3}	1.355	1.807
μ/mm^{-1}	0.558	1.525
data/restraints/ parameters	9729/0/412	10385/1/787
R_{int}	0.0402	0.0612
final R indices	R_1 = 0.0638	R_1 = 0.1108
$[I > 2\sigma I)]$	wR_2 = 0.1500	wR_2 = 0.2779
final R indices	R_1 = 0.0980	R_1 = 0.1346
(all data)	wR_2 = 0.1749	wR_2 = 0.2945

Table 2. Selected Distances for Compounds (PPN)-1 and (PPN)-2·CH_3CN

bonds	(PPN)-1	(PPN)-2·CH_3CN
Ni−S	Ni−S1 2.168(2)	Ni−S7 2.144(2)
	Ni−S2 2.176(2)	Ni−S8 2.149(2)
C−S	C10−S1 1.724(2)	C1−S7 1.668(2)
	C11−S2 1.715(2)	C2−S8 1.684(2)
C−C	C10−C11 1.547(2)	C1−C2 1.547(2)
C−O	C10−O2 1.216(2)	C1−O13 1.243(2)
	C11−O1 1.224(2)	C2−O14 1.250(2)
Mo−O		Mo3−O14 2.618(2)
		Mo2−O14 2.562(2)
		Mo1−O13 2.596(2)
		Mo6−O13 2.597(2)

The six $[Mo_2S_2O_2]^{2+}$ building blocks are connected through double hydroxo bridging ligands, which span nonbonding Mo−Mo contacts (3.344(2)−3.358(2)Å) alternating with short Mo−Mo bonding contacts within the building blocks (2.845(2)−2.851(2) Å) as usually observed for oxothiomolybdenum rings.[27,31−33,35,43] The $[Mo_{12}O_{12}S_{12}(OH)_{12}(Ni(dto)_2)]^{2-}$ cluster retains a D_{2h} idealized symmetry where the plane of the Mo_{12} ring contains the planar $[Ni(dto)_2]^{2-}$ complex (see side view of **2** in Figure 2b). The two peripheral oxalato groups of the guest are symmetrically anchored to the inorganic host with Mo−O distances in the 2.562(2)−2.618(2) Å range, each oxygen atom bridging two adjacent Mo atoms. These distances are much longer than those usually observed with other carboxylate guests (about 2.25−2.45 Å) and even longer than those

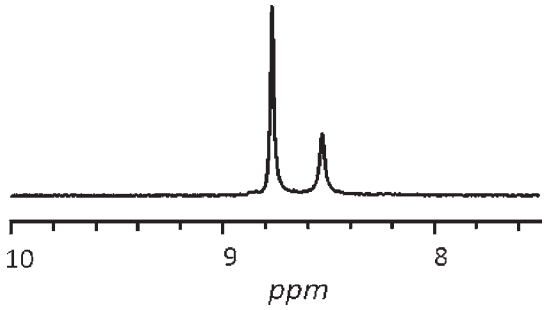

Figure 3. ^{1}H NMR spectra of **2** in CD_3CN showing the bridging hydroxo signals of the molybdenum ring.

observed in the $[Mo_8O_8S_8(OH)_8(C_2O_4)]^{2-}$ compound (Mo−O = 2.461(2)−2.559(2) Å).[35] These long distances suggest that the $[Ni(dto)_2]^{2-}$ complex is coordinated less strongly than the other guests studied previously, and these contacts between the host and the guest can be considered on the frontier between coordination and supramolecular chemistry. Consequently, eight Mo atoms display an octahedral environment, while the other four exhibit a square pyramidal geometry (the Mo···S distances involving the dto^{2-} ligands being too long to give coordination bonds). Interestingly, the encapsulation of $[Ni(dto)_2]^{2-}$ within the Mo_{12} ring provokes significant variations of the bond lengths of the complex. As shown in Table 2, the C−O bond lengths increase significantly from about 1.22 Å in **1** to 1.25 Å in **2**, whereas the C−S bonds appear slightly stronger (1.72 Å on average in **1** to 1.67 Å for **2**). Furthermore, the Ni−S bond lengths appear also affected by the encapsulation within the Mo_{12} and shorten weakly from 2.172(2) to 2.146(2) Å on average. Such variations are commonly observed when additional metals are coordinated to peripheral available carbonyl groups and characterizes a partial charge delocalization away from the sulfur atoms toward the additional coordinated electrophilic metals, that is, Mo(V).[4,8,9]

Infrared Spectra. FT-IR spectra of compounds **K-1** and **Rb-2** are depicted in Figure S1 (Supporting Information). The spectrum of **K-1** fully agrees with the "red" form of the complex $K_2[Ni(dto)_2]$ reported in the literature.[7,44,45] The IR spectrum of **Rb-2** contrasts with the spectrum of **K-1**. The strong absorptions observed at 960 and 515 cm^{-1} correspond to the fingerprint of the inorganic oxothiomolybdenum wheels.[43,46] Regarding the $[Ni(dto)_2]^{2-}$ moiety, the bathochromic shift of the C═O stretching frequency from 1594 and 1580 cm^{-1} to 1529 and 1513 cm^{-1} is usually observed in oxothiomolybdenum wheels templated by polycarboxylate ligands[31−35] and is, therefore, consistent with the host−guest structure. In addition, the hypsochromic shift of the $\nu_{(C-C)} + \nu_{(C-S)}$ combination band from 1085 to 1080 to 1102 cm^{-1} reflects the delocalization of charge toward the Mo-ring moiety, which results in a reduction of the C−O bond order and a decrease in the C−S bond length, consistent with X-ray data.

Proton NMR Spectra in Solution. The ^{1}H NMR spectrum of $[Mo_{12}(Ni(dto)_2)]^{2-}$ (**Rb-2**) in CD_3CN or in DMSO at room temperature (Figures 3 and S2 (Supporting Information), respectively) consists of two signals at 8.77 and 8.53 ppm in CD_3CN and at 10.85 and 10.69 ppm in DMSO with integration 8:4, respectively. These signals are consistent with structural data and are attributed to the 12 hydroxo bridges in $[Mo_{12}(Ni(dto)_2)]^{2-}$ in a D_{2h} symmetry. The two singlets are

dx.doi.org/10.1021/ic201239y |*Inorg. Chem.* 2011, 50, 9031–9038

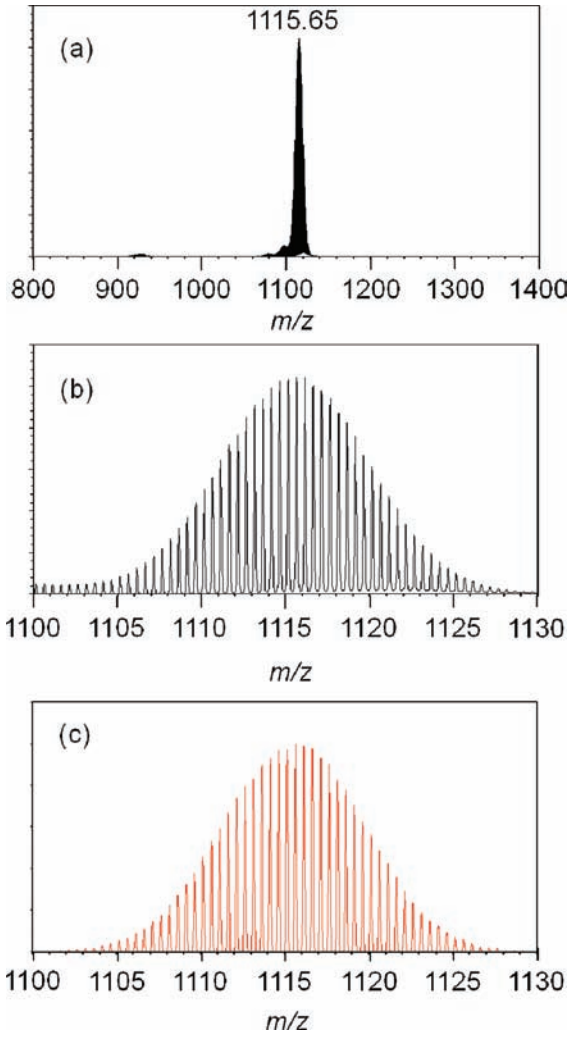

Figure 4. ESI-HRMS spectrum of **PPN-2** in CH_3CN. Full spectrum (a) and zoom in of the 1100−1130 m/z range (b). Theoretical spectrum calculated for the $[Mo_{12}O_{12}S_{12}(OH)_{12}(Ni(dto)_2)]^{2-}$ anion (c).

assigned to the eight "corner" hydroxo bridges (O7 to O10) and the four "edge" hydroxo groups (O11 and O12), respectively.

ESI-HRMS. During the past decade, mass spectrometry became a powerful analytic tool for the characterization of multicharged species, such as polyoxometalates.[47−54] In the present study, the ESI-HRMS spectrum of **PPN-2·CH$_3$CN** in acetonitrile (6×10^{-6} M) was recorded in the negative ion mode. As depicted in Figure 4a, the ESI-HRMS spectrum of **2** exhibits only one signal at m/z = 1115.6509. This peak is unambiguously attributed to the dicharged anion $[Mo_{12}O_{12}S_{12}(OH)_{12}(Ni(dto)_2)]^{2-}$, which gives the calculated value of m/z = 1115.6526. The expanded peak shown in Figure 4b matches perfectly with the calculated signal given in Figure 4c. The composition of the anion leads to a wide isotopic Gaussian distribution nicely resolved owing to the high resolution of the mass analyzer. Therefore, the high-resolution mass spectrum clearly confirms the nature and the stability of the anion **2** in acetonitrile even at low concentration.

Electronic Spectra. The electronic spectra of **1** (as **K-1** salt) and **2** (as **Rb-2** salt) in acetonitrile at the concentration of 2×10^{-4} mol·L^{-1} are depicted in Figure 5. The spectrum of **1** displays five maxima located at 228 (ε = 15 200 L·mol^{-1}·cm^{-1}), 264 (ε = 17 500 L·mol^{-1}·cm^{-1}), 305 (ε = 20 850 L·mol^{-1}·cm^{-1}), 502

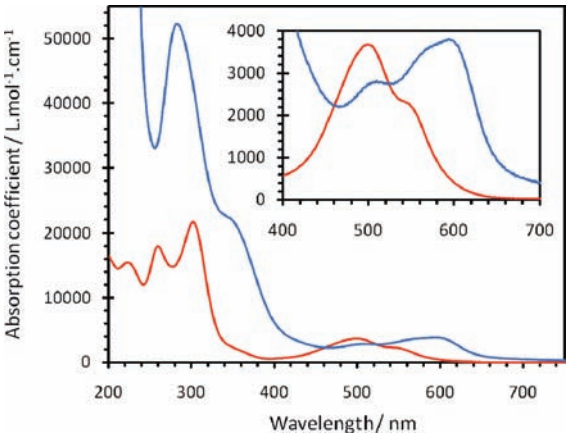

Figure 5. Electronic spectra of **K-1** (in red) and **Rb-2** (in blue) in CH_3CN for a concentration of 2×10^{-4} M. Inset: zoom in of the LMCT bands of the $[Ni(dto)_2]^{2-}$ moiety in **K-1** and **Rb-2**.

(ε = 3700 L·mol^{-1}·cm^{-1}), and 549 nm (ε = 2200 L·mol^{-1}·cm^{-1}). As previously reported, the three former bands are assigned to L(σ) → M, L(π) → L(π^*), and L(π) → M transitions, respectively, whereas the two latter correspond to an M → L(π^*) transition and to a combination between M → L(π^*) and d → d transitions, respectively.[45,55] Interestingly, the encapsulation of the complex **1** into the Mo_{12} ring results in a pronounced color change from pink for **1** to dark violet for **2**. This dramatic color change is accompanied by an important bathochromic shift of the M → L(π^*) charge-transfer bands that appear at 510 (ε = 2800 L·mol^{-1}·cm^{-1}), 571 (ε = 3600 L·mol^{-1}·cm^{-1}), and 597 nm (ε = 3800 L·mol^{-1}·cm^{-1}). This feature is characteristic of the coordination of the peripheral carbonyl groups to transition metals and was already reported when $[M^{II}(dto)_2]^{2-}$ (M^{II} = Ni, Pd, Pt, Cu) is coordinated to two alkyl tin cations.[56] In addition, **2** displays two important absorptions located at 284 nm (ε = 52 000 L·mol^{-1}·cm^{-1}) and 350 nm (ε = 21 800 L·mol^{-1}·cm^{-1}), characteristic of the Mo rings. Such intense absorptions correspond to E → Mo charge-transfer bands (LMCT) with E = S or O of the oxothio $\{Mo_2O_2S_2\}$ building blocks.[28,43] For instance, the electronic spectra of the $[Mo_8O_8S_8(OH)_8(C_2O_4)]^{2-}$ anion in DMF exhibits absorption at 280 nm (ε = 28 100 L·mol^{-1}·cm^{-1} and 350 nm (7600 L·mol^{-1}·cm^{-1}). In summary, the comparison of electronic spectra of **K-1** and **Rb-2** evidences a strong modification of the M → L(π^*) charge-transfer bands of $[Ni(dto)_2]^{2-}$ upon encapsulation within the Mo cycle in relationship with the observed structural changes.

Stability Studies. Prior to electrochemical studies, the stability of 2×10^{-4} mol·L^{-1} solutions of **K-1** and **Rb-2** was studied in acetonitrile by UV−visible spectroscopy. In both cases, the obtained spectra remained identical during several weeks, suggesting that **K-1** and **Rb-2** are perfectly stable under such conditions. These results are supported by ^{1}H NMR and ESI-HRMS studies.

The stability of the compounds **K-1** and **Rb-2** in CH_3CN acidic solutions was checked by UV−visible titration of 2×10^{-4} mol·L^{-1} solution by CF_3COOH (TFA) for the concentration ratio R = TFA/**2** or **1** ranging from 0 to 15. For the complex **1**, the stability in solution in the presence of acid was evidenced for the ratio R = TFA/**1** ranging from 0 to 15. Conversely, for **2**, no modification of the electronic spectra was observed until R = 5, whereas solutions turned slowly to yellow within some days for

dx.doi.org/10.1021/ic201239y |*Inorg. Chem.* 2011, 50, 9031–9038

higher ratios. ESI-HRMS studies performed on the same samples reveal an additional peak at m/z = 688.1, characteristic of the degradation of $[Mo_{12}O_{12}S_{12}(OH)_{12}(Ni(dto)_2)]^{2-}$ into $[Mo_8O_8S_8(OH)_8(Ox)]^{2-}$ for a TFA/**2** ratio higher than 5. Finally, no protonated species was identified for **2** by this technique, whatever the ratio R.

Electrochemical Studies. The cyclic voltammograms (CVs) of **1** (as **K-1** salt, 2.5×10^{-4} mol·L^{-1}) and **2** (as **Rb-2** salt, 10^{-4} mol·L^{-1}), recorded at a static glassy carbon working electrode in a dry acetonitrile solution containing 0.1 M NBu_4PF_6 as electrolyte, are shown in Figure S3 (Supporting Information). The CV of **1** displays two monoelectronic irreversible waves. Despite the fact that these waves are ill-defined, one can observe a reductive irreversible event around E_{pc} = −1.7 V vs Ag/AgCl attributed to the Ni^{II}/Ni^{I} couple and an irreversible oxidation process of Ni^{II} into Ni^{III} located at E_{pa} = ca. +0.6 V vs Ag/AgCl, in agreement with the literature data for similar complexes containing a $\{NiS_4\}$ core.[25,26,57−59] The cyclic voltammogramm of **2** exhibits the same pattern, but the reduction and oxidation waves are significantly shifted toward more positive potentials. The reductive irreversible process of **2** is centered around E_{pc} = −0.9 V vs Ag/AgCl and likely contains a contribution arising from the reduction of some Mo(V) centers of the ring.[27] The oxidation process associated with the Ni^{III}/Ni^{II} couple in **2** remains irreversible and is located at E_{pa} = +1.0 V vs Ag/AgCl. The positive shifts of reduction and oxidation potentials of the $[Ni(dto)_2]^{2-}$ moiety between **1** and **2** are related to a significant electronic effect induced by the capture of $[Ni(dto)_2]^{2-}$ within the oxothiomolybdenum wheel and can be explained in terms of withdrawing of the electronic density toward the Mo-ring moiety, in agreement with X-ray diffraction, FT-IR, and UV−visible studies.

Electrocatalytic Properties. Figures 6 and 7 show the cyclic voltammograms of **1** and **2** in CH_3CN + 0.1 M $(NBu_4)(PF_6)$, upon stepwise additions of TFA (pK_a = 12.7 in CH_3CN).[60]

The addition of increasing amounts of TFA in a solution of **1** leads to the growing of a new composite cathodic wave that moves from −1.30 V for R = 4.28 to −1.42 V vs Ag/AgCl for R = 8.56 and remains at that position as further acid equivalents are added. This wave rises in height when the ratio R increases, and the plot of the current intensity of the catalytic wave located at around −1.4 V as a function of R gives a linear behavior, consistent with an electrocatalytic behavior for the reduction of protons.[25,26,28,61]

The behavior of the compound **2** in CH_3CN in the presence of TFA is depicted in Figure 7. As the ratio R = TFA/**2** increases, a new cathodic event appears at an average value around −1.2 V vs Ag/AgCl. The intensity of this new cathodic peak increases linearly with the ratio R (inset, Figure 7) and shifts gradually toward more negative potentials (about 0.06 V per R unit). This reduction process is accompanied by the formation of bubbles on the surface of the electrode for R values above 10. We thus assigned this wave to an electrocatalytic behavior for the reduction of protons and evolution of dihydrogen gas.[25] In the course of a bulk electrolysis experiment of TFA carried out in CH_3CN (Figure S4, Supporting Information), the addition of **Rb-2** as an electrocatalyst clearly triggers the increase of the cathodic current that remains stable over the time of the experiment. However, in this experiment, we did not succeed in fully solubilizing **Rb-2** in the supporting electrolyte. We thus prepared a 10^{-4} M solution of **Rb-2** to which the supporting electrolyte and CF_3COOH (1.5 mM) were added. The evolution of the charge passed through the electrode during electrolysis of this solution at

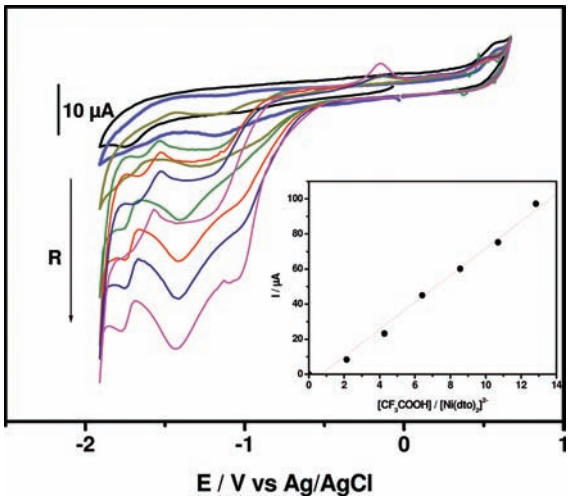

Figure 6. Cyclic voltammograms of **1** (2.5×10^{-4} M in CH_3CN + 0.1 M Bu_4NPF_6 as electrolyte) in the absence and presence of trifluoroacetic acid. The arrow indicates the increasing values of the ratio R = TFA/**1** (from R = 0 to R = 2.1, 4.3, 6.4, 8.6, 10.7, and 12.8). CVs are recorded at a glassy carbon electrode (GCE). Scan rate = 0.1 V s^{-1}. Potentials are given vs AgCl/Ag electrode. Inset: linear dependence of the catalytic current with the ratio R = TFA/**1**.

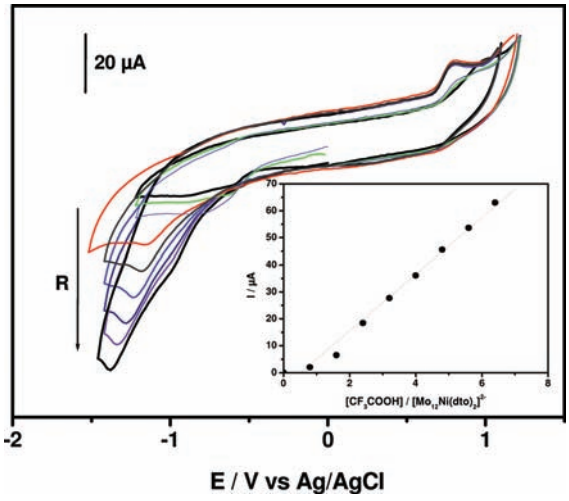

Figure 7. Cyclic voltammograms of **2** (10^{-4} M in CH_3CN + 0.1 M Bu_4NPF_6 as electrolyte) in the absence and presence of trifluoroacetic acid TFA. The arrow indicates the increasing values of the ratio R = TFA/**2** (from R = 0 to R = 0.8, 1.6, 2.4, 3.2, 4.8, 5.6, 6.4). CVs are recorded at a glassy carbon electrode (GCE). Scan rate = 0.1 V s^{-1}. Potentials are given vs AgCl/Ag electrode. Inset: linear dependence of the catalytic current with the ratio R = TFA/**2**.

−1.4 V vs Ag/AgCl, together with the control experiment carried out in the absence of **2**, allowed evidencing that hydrogen gas is evolved in both experiments, as indicated by gas chromatography monitoring. Unfortunately, because of the low solubility of **2**, the degradation of **2** during the electrolysis, and the detection limit of our setup, we could not decorrelate direct reduction of TFA at the electrode from catalytic H_2 evolution catalyzed by **2**.

Catalytic hydrogen evolution has already been observed with other thiomolybdic molecular clusters, such as oxothiomolybdenum wheels either in DMF[28] or in water,[27] the dinuclear complex $[Mo^{IV}_2(\mu\text{-}S)_2(Cp)_2(S-CH_2-S)]$ in CH_3CN,[62] or the trimetallic

compound $[Mo^{IV}_3S_4(nta)_3]^{5-}$ in aqueous media.[63] In the case of **2**, the half-wave potential of the electrocatalytic process (−1.0 V vs Ag/AgCl) in the presence of TFA in the millimolar range in CH_3CN allows determining an overpotential requirement of ∼0.6 V for H_2 evolution.[60] This value compares well with those observed for Ni-based bioinspired catalysts ranging between ∼0.6[19] and 1 V[25] and opens interesting perspectives for this class of compounds.

CONCLUSION

A new oxothiomolybdenum cycle formed around the $[Ni(dto)_2]^{2-}$ was discovered and characterized either in the solid state or in solution. It corresponds to the first example of a 3d transition-metal complex embedded in the plane of a Mo ring, and electrochemical studies evidenced that $[Ni(dto)_2]^{2-}$ and $[Mo_{12}(Ni(dto)_2)]^{2-}$ compounds are capable of reducing protons. The possibility to cumulate properties at the molecular level within such multicomponents systems gives promising perspectives to these preliminary results for the fine-tuning of the electrochemical reactivity. In particular, other cations, relevant for their electrochemical properties, give square-planar or square-based pyramidal complexes with dithiooxalato ligands, such as Cu(II),[9,64] Pt(II),[9,45,55] Pd(II),[9,45,55] Au(III),[55] $[FeNO]^{2+}$,[65] $[Mo{=}O]^{2+}$,[66] $[Tc{=}O]^{3+}$,[67] $[Re{=}O]^{3+}$,[67] or $[Mo_2O_2S_2]^{2+}$,[68,69] and offer a wide range of possible electroactive compounds. This work is currently in progress.

ASSOCIATED CONTENT

Supporting Information. Experimental details, FT-IR spectra (Figure S1), NMR spectra in DMSO and in CD_3CN (Figure S2), cyclo-voltamograms of **1** and **2** in CH_3CN without addition of acid (Figure S3), bulk electrolysis experiment of TFA in CH_3CN before and after addition of **2** (Figure S4), and X-ray crystallographic data in CIF format. This material is available free of charge via the Internet at http://pubs.acs.org.

AUTHOR INFORMATION

Corresponding Author
*E-mail: sebastien.floquet@chimie.uvsq.fr.

ACKNOWLEDGMENT

We gratefully acknowledge the Centre National de la Recherche Scientifique (CNRS) and the Ministère de l'Enseignement Supérieur et de la Recherche (MESR) for their financial support. This work is supported by the French National Research Agency (ANR) under the contracts POMEAH·ANR-08-JCJC-0097 and NG2M·ANR-06-BLAN-0019 and C'Nano Ile de France through the project ECOPOMs 2009. Ms. Estelle Galmiche, from Versailles, is also acknowledged for ESI-HRMS measurements.

REFERENCES

(1) Jones, H. O.; Robinson, C. S. *J. Chem. Soc.* **1912**, *101*, 932–935.
(2) Robinson, C. S.; Jones, H. O. *J. Chem. Soc.* **1912**, *101*, 62–76.
(3) Jones, H. O.; Tasker, H. S. *J. Chem. Soc.* **1909**, *95*, 1904–1909.
(4) Coucouvanis, D.; Baenziger, N. C.; Johnson, S. M. *J. Am. Chem. Soc.* **1973**, *95*, 3875–3886.
(5) Coucouvanis, D. *J. Am. Chem. Soc.* **1970**, *92*, 707–709.
(6) Leitheiser, M.; Coucouvanis, D. *Inorg. Chem.* **1977**, *16*, 1611–1614.
(7) Coucouvanis, D.; Piltingsrud, D. *J. Am. Chem. Soc.* **1973**, *95*, 5556–5563.
(8) Gleizes, A.; Verdaguer, M. *J. Am. Chem. Soc.* **1981**, *103*, 7373–7374.
(9) Gleizes, A.; Verdaguer, M. *J. Am. Chem. Soc.* **1984**, *106*, 3727–3737.
(10) Frasse, C.; Trombe, J. C.; Gleizes, A.; Galy, J. *C. R. Acad. Sci., Ser. II* **1985**, *300*, 403–406.
(11) Trombe, J. C.; Gleizes, A.; Galy, J. *C. R. Acad. Sci., Ser. II* **1982**, *294*, 1369–1372.
(12) Gleizes, A.; Maury, F.; Cassoux, P.; Galy, J. *Z. Kristallogr.* **1981**, *155*, 293–306.
(13) Bradley, J. M.; Carling, S. G.; Visser, D.; Day, P.; Hautot, D.; Long, G. J. *Inorg. Chem.* **2003**, *42*, 986–996.
(14) Decurtins, S.; Schmalle, H. W.; Pellaux, R.; Schneuwly, P.; Hauser, A. *Inorg. Chem.* **1996**, *35*, 1451–1460.
(15) Artero, V.; Fontecave, M. *Coord. Chem. Rev.* **2005**, *249*, 1518–1535.
(16) Verhagen, J. A. W.; Lutz, M.; Spek, A. L.; Bouwman, E. *Eur. J. Inorg. Chem.* **2003**, 3968–3974.
(17) Ohki, Y.; Tatsumi, K. *Eur. J. Inorg. Chem.* **2011**, 973–985.
(18) Barton, B. E.; Rauchfuss, T. B. *J. Am. Chem. Soc.* **2010**, *132*, 14877–14885.
(19) Canaguier, S.; Fontecave, M.; Artero, V. *Eur. J. Inorg. Chem.* **2011**, 1094–1099.
(20) Vaccaro, L.; Artero, V.; Canaguier, S.; Fontecave, M.; Field, M. J. *Dalton Trans.* **2010**, *39*, 3043–3049.
(21) Canaguier, S.; Field, M.; Oudart, Y.; Pecaut, J.; Fontecave, M.; Artero, V. *Chem. Commun.* **2010**, *46*, 5876–5878.
(22) Oudart, Y.; Artero, V.; Norel, L.; Train, C.; Pecaut, J.; Fontecave, M. *J. Organomet. Chem.* **2009**, *694*, 2866–2869.
(23) Canaguier, S.; Vaccaro, L.; Artero, V.; Ostermann, R.; Pecaut, J.; Field, M. J.; Fontecave, M. *Chem.—Eur. J.* **2009**, *15*, 9350–9364.
(24) Canaguier, S.; Artero, V.; Fontecave, M. *Dalton Trans.* **2008**, 315–325.
(25) Oudart, Y.; Artero, V.; Pecaut, J.; Fontecave, M. *Inorg. Chem.* **2006**, *45*, 4334–4336.
(26) Angamuthu, R.; Bouwman, E. *Phys. Chem. Chem. Phys.* **2009**, *11*, 5578–5583.
(27) Duval, S.; Floquet, S.; Simonnet-Jégat, C.; Marrot, J.; Biboum, R. N.; Keita, B.; Nadjo, L.; Haouas, M.; Taulelle, F.; Cadot, E. *J. Am. Chem. Soc.* **2010**, *132*, 2069–2077.
(28) Keita, B.; Floquet, S.; Lemonnier, J. F.; Cadot, E.; Kachmar, A.; Bénard, M.; Rohmer, M. M.; Nadjo, L. *J. Phys. Chem. C* **2008**, *112*, 1109–1114.
(29) Cadot, E.; Pouet, M. J.; Robert-Labarre, C. R.; du Peloux, C.; Marrot, J.; Sécheresse, F. *J. Am. Chem. Soc.* **2004**, *126*, 9127–9134.
(30) Dolbecq, A.; Cadot, E.; Sécheresse, F. *Chem. Commun.* **1998**, 2293–2294.
(31) Lemonnier, J. F.; Kachmar, A.; Floquet, S.; Marrot, J.; Rohmer, M. M.; Bénard, M.; Cadot, E. *Dalton Trans.* **2008**, 4565–4574.
(32) Lemonnier, J. F.; Floquet, S.; Marrot, J.; Terazzi, E.; Piguet, C.; Lesot, P.; Pinto, A.; Cadot, E. *Chem.—Eur. J.* **2007**, *13*, 3548–3557.
(33) Lemonnier, J. F.; Floquet, S.; Kachmar, A.; Rohmer, M. M.; Bénard, M.; Marrot, J.; Terazzi, E.; Piguet, C.; Cadot, E. *Dalton Trans.* **2007**, 3043–3054.
(34) Floquet, S.; Marrot, M.; Cadot, E. *C. R. Chim.* **2005**, *8*, 1067–1075.
(35) Salignac, B.; Riedel, S.; Dolbecq, A.; Sécheresse, F.; Cadot, E. *J. Am. Chem. Soc.* **2000**, *122*, 10381–10389.
(36) Cadot, E.; Marrot, J.; Sécheresse, F. *Angew. Chem., Int. Ed.* **2001**, *40*, 774–777.
(37) Keita, B.; Nadjo, L. *J. Electroanal. Chem.* **1988**, *243*, 87–103.
(38) Cadot, E.; Salignac, B.; Marrot, J.; Dolbecq, A.; Sécheresse, F. *Chem. Commun.* **2000**, 261–262.
(39) Cox, E. G.; Sharratt, E.; Wardlaw, W.; Webster, K. C. *J. Chem. Soc.* **1936**, 129–133.
(40) Cox, E. G.; Wardlaw, W.; Webster, K. C. *J. Chem. Soc.* **1935**, 1475–1480.

(41) Benedix, R.; Hofbauer, M.; Mobius, M.; Knoch, F. *Inorg. Chim. Acta* **1997**, *262*, 177–185.
(42) Trombe, J. C.; Gleizes, A.; Galy, J. 1985, *300*, 5−8.
(43) Lemonnier, J. F.; Floquet, S.; Marrot, J.; Cadot, E. *Eur. J. Inorg. Chem.* **2009**, 5233–5239.
(44) Czernuszewicz, R. S.; Nakamoto, K.; Strommen, D. P. *J. Am. Chem. Soc.* **1982**, *104*, 1515–1521.
(45) Roman, P.; Beitia, J. I.; Luque, A.; Guzmanmiralles, C. *Polyhedron* **1995**, *14*, 1091–1096.
(46) Lemonnier, J. F.; Floquet, S.; Marrot, J.; Cadot, E. *J. Cluster Sci.* **2006**, *17*, 267–282.
(47) Mayer, C. R.; Fournier, I.; Thouvenot, R. *Chem.—Eur. J.* **2000**, *6*, 105–110.
(48) Sokolov, M. N.; Korenev, V. S.; Izarova, N. V.; Peresypkina, E. V.; Vicent, C.; Fedin, V. P. *Inorg. Chem.* **2009**, *48*, 1805–1807.
(49) Song, Y. F.; Long, D. L.; Kelly, S. E.; Cronin, L. *Inorg. Chem.* **2008**, *47*, 9137–9139.
(50) Micoine, K.; Hasenknopf, B.; Thorimbert, S.; Lacote, E.; Malacria, M. *Org. Lett.* **2007**, *9*, 3981–3984.
(51) Miras, H. N.; Wilson, E. F.; Cronin, L. *Chem. Commun.* **2009**, 1297–1311.
(52) Yan, J.; Gao, J.; Long, D. L.; Miras, H. N.; Cronin, L. *J. Am. Chem. Soc.* **2010**, *132*, 11410–11411.
(53) Wilson, E. F.; Abbas, H.; Duncombe, B. J.; Streb, C.; Long, D. L.; Cronin, L. *J. Am. Chem. Soc.* **2008**, *130*, 13876–13884.
(54) Ritchie, C.; Burkholder, E. M.; Long, D. L.; Adam, D.; Kogerler, P.; Cronin, L. *Chem. Commun.* **2007**, 468–470.
(55) Latham, A. R.; Hascall, V. C.; Gray, H. B. *Inorg. Chem.* **1965**, *4*, 788–792.
(56) Coucouvanis, D.; Coffman, R. E.; Piltingsrud, D. *J. Am. Chem. Soc.* **1970**, *92*, 5004–5006.
(57) Saito, G.; Izukashi, H.; Shibata, M.; Yoshida, K.; Kushch, L. A.; Kondo, T.; Yamochi, H.; Drozdova, O. O.; Matsumoto, K.; Kusunoki, M.; Sakaguchi, K.; Kojima, N.; Yagubskii, E. B. *J. Mater. Chem.* **2000**, *10*, 893–910.
(58) Saito, G.; Yoshida, K.; Shibata, M.; Yamochi, H.; Kojima, N.; Kusunoki, M.; Sakaguchi, K. *Synth. Met.* **1995**, *70*, 1205–1208.
(59) Verhagen, J. A. W.; Ellis, D. D.; Lutz, M.; Spek, A. L.; Bouwman, E. *J. Chem. Soc., Dalton Trans.* **2002**, 1275–1280.
(60) Fourmond, V.; Jacques, P. A.; Fontecave, M.; Artero, V. *Inorg. Chem.* **2010**, *49*, 10338–10347.
(61) Le Goff, A.; Artero, V.; Jousselme, B.; Tran, P. D.; Guillet, N.; Metaye, R.; Fihri, A.; Palacin, S.; Fontecave, M. *Science* **2009**, *326*, 1384–1387.
(62) Appel, A. M.; DuBois, D. L.; Rakowski-DuBois, M. *J. Am. Chem. Soc.* **2005**, *127*, 12717–12726.
(63) Shibahara, T.; Yamasaki, M.; Sakane, G.; Minami, K.; Yabuki, T.; Ichimura, A. *Inorg. Chem.* **1992**, *31*, 640.
(64) Coucouvanis, D. *J. Am. Chem. Soc.* **1971**, *93*, 1786–1788.
(65) Qian, L.; Singh, P.; Ro, H.; Hatfield, W. E. *Inorg. Chem.* **1990**, *29*, 761–763.
(66) Mennemann, K.; Mattes, R. *J. Chem. Res., Synop.* **1979**, 102.
(67) Davison, A.; Orvig, C.; Trop, H. S.; Sohn, M.; DePamphilis, B. V.; Jones, A. G. *Inorg. Chem.* **1980**, *19*, 1988–1992.
(68) Mennemann, K.; Mattes, R. *J. Chem. Res., Synop.* **1979**, 100–101.
(69) Coucouvanis, D.; Toupadakis, A.; Hadjikyriacou, A. *Inorg. Chem.* **1988**, *27*, 3272–3273.